EFFECT OF HYDRIDING ON NANOSCALE PLASTICITY MECHANISMS IN NANOCRYSTALLINE PALLADIUM THIN FILMS

Behnam Amin-Ahmadi, EMAT, University of Antwerp, Belgium
behnam.amin-ahmadi@uantwerpen.be
Hosni Idrissi, EMAT, University of Antwerp, Belgium; Marc Fivel, University of Grenoble, France; Renaud Delmelle, Université catholique de Louvain, Belgium; Stuart Turner, EMAT, University of Antwerp, Belgium; Thomas Pardoen, Université catholique de Louvain, Belgium; Joris Proost, Université catholique de Louvain, Belgium; Dominique Schryvers, EMAT, University of Antwerp, Belgium

Thin palladium (Pd) membranes constitute an enabling material in hydrogen permeation and sensing applications. During hydriding of Pd, as long as the H/Pd (atomic ratio) stays below $\alpha_{SSmax} \approx 0.02$, the α-Pd with face centered cubic (fcc) lattice will expand from 3.889 Å to 3.895 Å. When the ratio reaches 0.02 a β-phase, again fcc based, having a lattice constant near 4.025 Å appears which induces a 10% volume change. In the present work, nanoscale plasticity mechanisms activated in sputtered nanocrystalline (nc) Pd thin films subjected to hydriding at different hydrogen pressures have been investigated for the first time using advanced TEM. The in-situ measurement of the evolution of the internal stress during hydriding shows that the internal stress increases rapidly and reaches a constant value of 120 MPa tensile stress for α phase and 920 MPa compressive stress for β phase transformation. The automated crystallographic orientation mapping in TEM (ACOM-TEM) before and after hydriding to α and β phase did not reveal significant changes of the grain size and the crystallographic texture, excluding grain boundary mediated processes as dominant hydrogen induced plasticity mechanisms. High resolution TEM (HRTEM) investigation of ∑3 {111} coherent twin boundaries (TBs) in Pd films shows clear loss of the coherency of these boundaries after hydriding to β phase. However, significant changes of microstructure have not been observed in Pd films hydrated to α phase. These results confirm that hydrogen induced plasticity is mainly controlled by dislocation activity at higher hydrogen pressures. Surprisingly, an fcc→9R phase transformation at Σ3 {112} incoherent TBs as well as a high density of stacking faults (SFs) (Fig. 1a) have been observed after hydriding to β phase indicating a clear effect of hydrogen on the stacking fault energy of Pd. Shear type faulted loops rarely reported in nc materials were also observed within the Pd grains after hydriding to β-phase (Fig. 1b). In order to investigate the stability of this shear type loops, different internal stress fields originating from the neighboring dislocation (dislocation "d3") and surface effects (image forces) have been computed using a Finite Element method (Fig. 1c). Such calculations confirm that high attractive forces exist between the dislocation “d2” and “d3” forming the dipole. On the other hand, although the Peach Koehler force on the dislocation “d1” tends to extend the SF, the force magnitude is much smaller than the force induced by the fault on the partial segments. Therefore, an extra shear stress of +385MPa ($\tau_{dis.}$) acting on the glide plane of the dislocation “d1” is required in order to counter balance the attractive force of the SF which thus explains the stability of this dislocation in the TEM thin foil after dehydriding. This shear stress can not be compensated by the negligible image force in such thin foil. Moreover, no residual hydrides were detected using high resolution electron energy loss spectroscopy. Therefore, the stability of glissile intrinsic SF loops in nc Pd films after dehydriding can thus be attributed to the presence of large internal stress heterogeneities typical of nc materials.

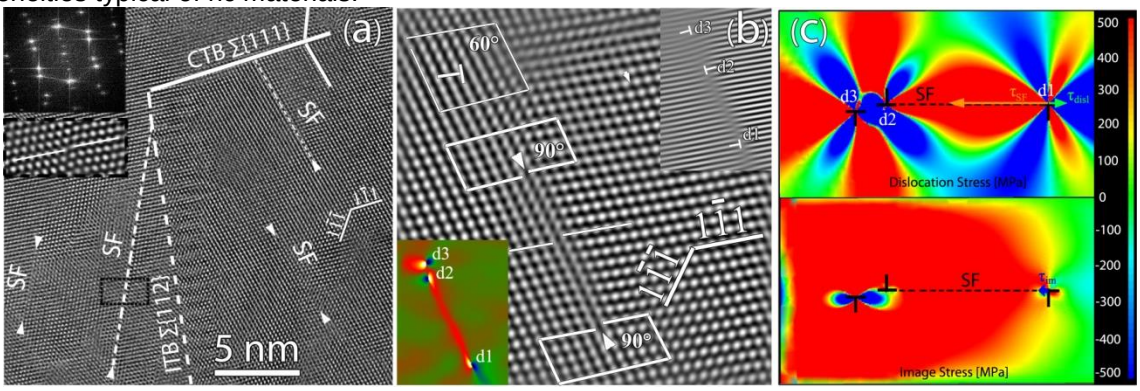

Figure 1 – After hydriding to β-phase: (a) [110] HRTEM image of a Pd nano-grain with the corresponding Fast Fourier Transform (FFT) pattern revealing twinning. Several SFs are indicated in the same figure by arrowheads. b) Enlarged Inverse FFT showing a SF loop with opposite 90° partial dislocations. Inverse FFT of (-111) plane and corresponding local g-map are shown in the upper right and lower left insets, respectively. c) Shear component of dislocations stress field and image internal stress fields. The arrows show the glide component of the Peach-Koehler force induced by the SF, the dislocations and the image stresses.